Radial Bright Channel Prior for Single Image Vignetting Correction

Hojin Cho, Hyunjoon Lee, and Seungyong Lee

Pohang University of Science and Technology (POSTECH), Korea

Abstract. This paper presents a novel prior, *radial bright channel (RBC) prior*, for single image vignetting correction. The RBC prior is derived from a statistical property of vignetting-free images: for the pixels sharing the same radius in polar coordinates of an image, at least one pixel has a high intensity value at some color channel. Exploiting the prior, we can effectively estimate and correct the vignetting effect of a given image. We represent the vignetting effect as an 1D function of the distance from the optical center, and estimate the function using the RBC prior. As it works completely in 1D, our method provides high efficiency in terms of computation and storage costs. Experimental results demonstrate that our method runs an order of magnitude faster than previous work, while producing higher quality results of vignetting correction.

Keywords: radial bright channel prior, vignetting correction.

1 Introduction

In vignetting correction, image degradation is usually modeled as:

$$Z(r,\theta) = I(r,\theta) \cdot V(r), \tag{1}$$

where Z and I respectively represent the input and latent vignetting-free image in polar coordinates whose origin is the optical center of the image, and V represents the 1D vignetting function assuming the vignetting is rotationally symmetric. The goal of image vignetting correction is to estimate both V and I from a single input Z, which is an under-constrained problem.

Various approaches have been proposed for solving the vignetting correction problem, by utilizing a predefined template based photometric calibration [12,1,6,13] and multiple images of different intensity attenuation [10,3,5,9]. Although these methods can remove vignettes effectively, they require reference calibration images or multiple input images with known camera settings. On the other hand, single image based approaches attempt to restore vignetting-free images without any additional information [15,17]. Such methods can produce high quality results for various images in a fully automatic fashion, but they involve heavy computations and thus may not be directly applicable for consumer products. Since vignetting is an undesired artifact in many computer vision applications, an effective and efficient vignetting correction method is still highly demanded.

D. Fleet et al. (Eds.): ECCV 2014, Part II, LNCS 8690, pp. 189–202, 2014.

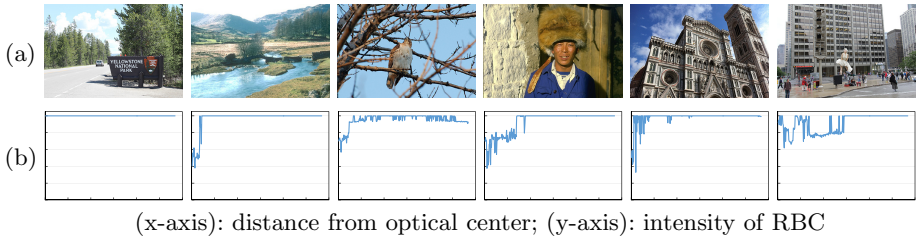

Fig. 1. Radial bright channel (RBC). (a) vignetting-free images. (b) RBC values corresponding to (a), which form almost horizontal lines except near the optical centers.

In this paper, we propose a novel prior, *radial bright channel (RBC) prior*, for single image vignetting correction. Similar to the dark channel prior [4], the RBC prior is derived from a statistical property of vignetting-free natural images: for the pixels sharing the same radius in polar coordinates of an image, there frequently exists at least one pixel (called *radial bright pixel*) such that its intensity is close to the maximum intensity of the image, except near the optical center (Fig. 1a). By arranging radial bright pixels with respect to the distances from the optical center, we can extract a 1D curve called *radial bright channel*, which is an almost *horizontal* line (Figs. 1b and 2b). If an image is affected by vignetting, then the overall image intensities radially fall off away from the optical center, affecting the intensities of the RBC as well (Fig. 2d). Thus, the RBC of an image can provide a rough approximation of the vignetting effect.

Based the RBC prior, we develop an effective vignetting estimation algorithm. Instead of using the whole image pixels, our method only uses a 1D RBC to estimate the vignetting profile, assuming the vignetting is rotationally symmetric. Consequently, the proposed algorithm is computationally and memory efficient and runs an order of magnitude faster than previous methods [15,11,17]. To handle potential outliers in an image (e.g., objects near the optical center and over-exposed pixels), our vignetting estimation algorithm involves an iterative refinement process that evaluates and rejects the outliers. Experimental results demonstrate that our method outperforms previous single image vignetting correction algorithms in terms of result quality and speed.

Our contributions are summarized as follows:

- Novel image prior, called *radial bright channel prior*, that can be used for accurately characterizing the vignetting effects.
- Fast and robust single image based vignetting estimation algorithm which runs in the 1D spatial domain using the radial bright channel prior.

2 Related Work

There are a variety of vignetting correction techniques in the literature. An intuitive approach to estimate the vignetting is to calibrate the camera using a

reference image taken under a uniform illumination [12,1,6,13]. This calibration-based approach can provide a plausible vignetting profile for known camera settings when the camera is available. However, the estimated vignettes would not correspond to images captured with different camera settings or lenses. This approach is barely suitable for arbitrary images downloaded from the internet.

Another related approach is to use multiple images taken with the same camera. In these methods, vignetting profiles are calibrated by utilizing overlapping views [10,7,3], different camera settings for exposure time and aperture [5], or a large number of images [9]. By considering the correspondence among multiple images with different intensity attenuations, ill-posedness of the vignetting problem can be reduced. However, this approach cannot be generally applied in practice as the corresponding multiple images are not often available.

Recently single image based vignetting correction has attracted more attention due to its flexibility [16,11,17]. An early approach in this category is based on image segmentation for classifying homogeneous regions with respect to color or texture, and estimates vignetting from intensity attenuation within each region [16]. This algorithm highly depends on image segmentation which is usually not robust for natural images, and is vulnerable to artifacts such as vignetting inconsistency between decomposed regions. A more sophisticated method utilizes the radial gradient symmetry of natural images [17]. This algorithm works well on a variety of natural images, but their asymmetry measure involves Kullback-Leibler divergence between positive and negative gradient distributions, which may not be robustly computed due to image noise and numerical instability. Similarly, inspired by [18,14] (the former version of [17]), statistical regularities of image derivatives have been exploited for vignetting correction [11], but there could be some ambiguity in the relationship between vignetting effects and image derivative distributions. Although several solutions exist for single image vignetting correction, they involve heavy computations due to nonlinear optimization with complicated priors for vignetting-free images.

3 Radial Bright Channel Prior

For a given image I, its radial bright channel (RBC) I^{RB} is formally defined as:

$$I^{\mathrm{RB}}(r) = \max_{\theta} \left\{ \max_{\mathcal{C}} I^{\mathcal{C}}(r, \theta) \right\}, \tag{2}$$

where r is the radial distance from the optical center, $\theta \in [0, 2\pi)$, $\mathcal{C} \in \{R, G, B\}$, and $I^{\mathcal{C}}$ is a color channel of I. For notational simplicity, we will omit the ranges of $\mathcal{C}$ and θ unless necessary. Fig. 2a illustrates how to compute $I^{\mathrm{RB}}(r)$ for an image. The RBC prior can be summarized as: for almost all r, $I^{\mathrm{RB}}(r)$ is close to the maximum channel value c_0 of an image, where $c_0 = \max_{r,\theta,\mathcal{C}} I^{\mathcal{C}}(r, \theta)$. That is, when we plot $I^{\mathrm{RB}}(r)$ with respect to r, the curve is an almost horizontal line with the value of c_0 (Fig. 2b).

The RBC prior is based on the statistical property we can observe from natural images. In an ordinary image, we can easily observe high intensities, mainly due

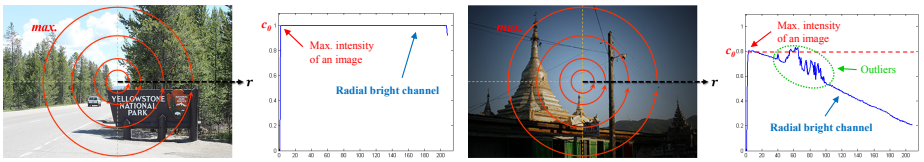

(a) (b) (c) (d)

Fig. 2. RBC Computation. (a, c) computation of $I^{\mathrm{RB}}(r)$ in the 2D spatial domain. (b, d) resulting RBCs.

to two factors: 1) bright objects/surfaces; 2) colorful objects/surfaces that cause high values at some color channels. For many images, large portions of image regions (e.g., sky, sea, and ground for an outdoor scene, and wall and window for indoor) are usually well lit by the sunlight or other kinds of illuminations, as shown in Fig. 1a. These well-lit regions would contain almost uniformly high intensity values in some color channels. If we draw relatively large circles centered at the image center as illustrated in Fig. 2a, then some parts of the circles should intersect those well-lit regions and the maximum intensities for the circles will come from the intersected parts. Thus the intensity uniformity of well-lit regions will bring us the RBC prior.

To validate our observation, we downloaded various kinds of images from flickr.com and manually picked out vignetting-free images with proper brightness since vignetting is not well perceived in dark images. Among them, 3,000 images were randomly selected and uniformly scaled so that the distance from the image center to the farthest boundary pixel becomes 500 pixels. Then, to investigate how similar I^{RB} is to the maximum channel value of an image, we computed $I^{residual} = c_0 - I^{\mathrm{RB}}$ for image pixels (see Fig. 2b). We did not use all values of $I^{residual}$ because many natural images contain objects (e.g., human) near the image center. In our experiment, we rejected the first 30% of the distance range $[0, 500]$ as outliers, considering that generally vignetting does not strongly affect the pixels near the image center. In addition, we ignored the pixels with intensity values above 240, since they could have been over-exposed.

Fig. 3a shows the normalized histogram of $I^{residual}$ obtained from the 3,000 images. The total number of pixel samples used for the histogram is about one million. We observe that about 88% of the pixels in the RBCs have values equal to c_0. Considering the error tolerance, we find 94.5% and 99.5% of the residual values are below five and 15, respectively. Fig. 3b shows another meaningful statistics that most of the images have almost zero mean residual values. With these observations, our RBC prior can be considered strong enough to be applied for a large portion of natural images. The RBCs estimated for various natural images are shown in Fig. 1b.

For an image with vignetting, on the other hand, the overall image brightness is attenuated radially from the optical center and the RBC deviates from the maximum channel value of the image. Interestingly, however, the RBC extracted from such an image well captures the overall distribution of the vignetting effects,

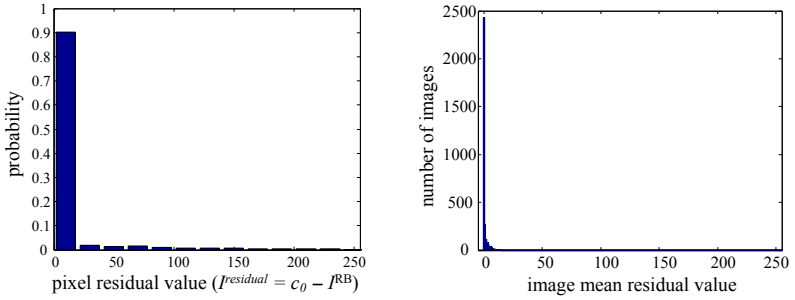

(a) (b)

Fig. 3. RBC statistics. (a) normalized histogram of the residual values from about one million sample pixels in 3,000 images. The width of each bin is 16 intensity levels. (b) histogram of the mean residual values of the 3,000 images.

as shown in Fig. 2d. This property motivates our vignetting correction method, and the detailed algorithm will be described in Sec. 4.

Implementation Details. Similar to most vignetting correction methods, we assume the optical center of an input image is located at the image center. To robustly compute RBCs, we quantize the distance r between a pixel and the image center to discrete values. For each discrete value r, color channel values of the pixels belonging to r are stored into a histogram of 256 bins. Considering outliers (e.g., noise and saturation) in an image, we check each bin in the histogram and reject it if the bin size is smaller than a predefined empirical threshold T. Then the maximum channel value for r is chosen from the remaining bins. In the experiments, we set $T = 0.01 \times W$ for all images, where W is the maximum of image width and height.

4 Vignetting Correction Using RBC Prior

Fig. 4 shows the overall process of our vignetting correction algorithm using the RBC prior. From a given input image Z whose color channel values are ranged between 0 and 1, we first compute the RBC Z^{RB}. The vignetting function is then estimated using our iterative optimization technique, and finally the vignette-free image I is recovered with the estimated vignetting function.

4.1 Simple Estimation of the Vignetting Function

As described in Sec. 3, the RBC of an image exhibits the overall profile of vignetting effects. To utilize the RBC for vignetting correction, we first derive from Eq. (1) a relationship between the RBC and the vignetting profile. Note that in this paper, we assume that vignetting is rotationally symmetric and its effects are the same over all color channels.

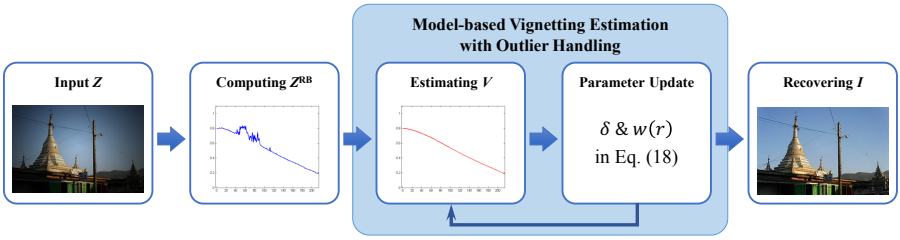

Fig. 4. Overview of our vignetting correction process

Taking two max operations over θ and color channels $\mathcal{C}$ in the image model of Eq. (1), we obtain

$$Z^{\mathrm{RB}}(r) = \max_{\theta} \left\{ \max_{\mathcal{C}} Z^{\mathcal{C}}(r,\theta) \right\} = \left[\max_{\theta} \left\{ \max_{\mathcal{C}} I^{\mathcal{C}}(r,\theta) \right\} \right] \cdot V(r), \tag{3}$$

as V is independent of θ and $\mathcal{C}$. Using Eq. (2), we have

$$Z^{\mathrm{RB}}(r) = I^{\mathrm{RB}}(r) \cdot V(r). \tag{4}$$

The statistics in Sec. 3 implies that I^{RB} is near constant with respect to r if we neglect outliers. Consequently, we can estimate the vignetting function V by substituting I^{RB} with a constant c_0 and minimizing the following term:

$$\arg\min_{V,c_0} \sum_{r=1}^{n} \left\| c_0 V(r) - Z^{\mathrm{RB}}(r) \right\|^2, \tag{5}$$

where V becomes equivalent to Z^{RB} if $c_0 = 1$. However, this naive estimation of V would be vulnerable to outliers in Z, such as objects near the image center, saturated pixels, image noise, and dark backgrounds (Fig. 5b). We propose a model based solution to robustly handle outliers in vignetting estimation.

4.2 Model-Based Vignetting Estimation with Outlier Handling

From Eq. (4), we formulate the joint probability of I^{RB} and V with respect to Z^{RB} as

$$p\left(I^{\mathrm{RB}}, V | Z^{\mathrm{RB}}\right) \propto p\left(Z^{\mathrm{RB}} | I^{\mathrm{RB}}, V\right) p\left(I^{\mathrm{RB}}, V\right). \tag{6}$$

To estimate V effectively and robustly in Eq. (6), we use a parametric representation for V by adopting the extended Kang-Weiss model [15]. In the Kang-Weiss model, a vignetting function is modeled with three factors: off-axis illumination

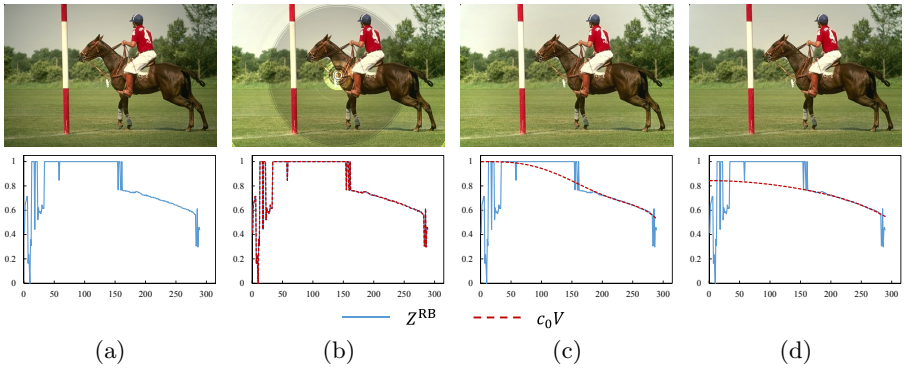

Fig. 5. Comparison of vignetting function estimation results. (a) input image. (b) naive estimation. (c) initial model-based estimation. (d) final model-based estimation with outlier handling. In (c), outliers in Z^{RB} near the image center are not properly filtered out, making the central region of the image darker than around the boundary. Such artifact is removed in (d) with our iterative refinement process.

factor A, geometric factor G, and tilt factor T. Among them, tilt factor is often ignored in practice and the vignetting function V is modelled as follows:

$$V(r) = A(r) \cdot G(r), \tag{7}$$

$$A(r) = \frac{1}{\{1 + (r/f)^2\}^2}, \tag{8}$$

$$G(r) = 1 - \sum_{i=1}^{p} \alpha_i \left(\frac{r}{n}\right)^p, \tag{9}$$

where f is the focal length of the camera and $\{\alpha_i\}$ are the coefficients of G.

By substituting I^{RB} with c_0 and plugging Eq. (7) into Eq. (6), we have

$$\begin{aligned} p\left(c_0, V | Z^{\mathrm{RB}}\right) &\propto p\left(Z^{\mathrm{RB}} | c_0, f, \{\alpha_i\}\right) p\left(c_0, f, \{\alpha_i\}\right) \\ &= p\left(Z^{\mathrm{RB}} | c_0, f, \{\alpha_i\}\right) p(c_0) p(f) \prod_{i=1}^{p} p(\alpha_i), \end{aligned} \tag{10}$$

with the assumption that all the model parameters are independent of each other. To estimate the parameters $\{c_0, f, \{\alpha_i\}\}$, we convert Eq. (10) into an energy function by taking negative log, and minimize the energy with some additional constraints:

$$\begin{aligned} \underset{c_0, f, \{\alpha_i\}}{\arg\min} \ & \lambda_d E_{data} + \lambda_{c_0} E_{c_0} + \lambda_f E_f + \lambda_\alpha \sum_{i=1}^{p} E_{\alpha_i}, \\ & \text{subject to} \ \ \forall_r V(r) \geq V(r+1) \ \ \text{and} \ \ 0 \leq c_0 \leq 1. \end{aligned} \tag{11}$$

Data Term. For the data term E_{data}, we utilize our RBC prior. Differently from Eq. (5), we use a truncated L_1 distance which is known to be more robust to outliers so that:

$$E_{data} = \sum_{r=1}^{n} w(r) \cdot \min\left(\left|c_0 V(r) - Z^{\mathrm{RB}}(r)\right|, \delta\right), \tag{12}$$

where w is a weight function. In modeling the weight function, it is important to give higher weights to the samples far from the optical center because vignetting appears more severely as r increases and Z^{RB} values near the optical center are unreliable. In our experiments, we tested several types of functions and found that a quadric function of r works well in most cases:

$$w(r) = \frac{r^2}{\sum_{r=1}^{n} r^2}. \tag{13}$$

In addition, we set the first 30% of w as zero to reject outliers near the optical center, as we did for computing the statistics in Sec. 3. w is updated during our optimization process to adaptively handle outliers in Z^{RB}, such as over-exposed pixels and pixels outside the image boundary.

Prior Terms. For computing E_{c_0}, we assume that c_0 is similar to the maximum value of Z^{RB} excluding outliers, and define

$$E_{c_0} = \left(\max(c_0 V|w) - \max(Z^{\mathrm{RB}}|w)\right)^2, \tag{14}$$

where $\max(c_0 V|w)$ is the maximum among the values of $c_0 V(r)$ for which $w(r) \neq 0$, and $\max(Z^{\mathrm{RB}}|w)$ is similarly defined.

To compute E_f, we use a well-known prior for the focal length [8] in which f is similar to the image size:

$$E_f = \left\{(W - f)/W\right\}^2, \tag{15}$$

where W is the maximum of the image width and height.

For E_{α_i}, we enforce all the values of α_i to remain small since the vignetting function V should be smooth across the image. We thus formulate E_{α_i} as:

$$E_\alpha = \alpha_i^2. \tag{16}$$

Constraints. The first constraint in Eq. (11) makes V monotonically decreasing, which is a natural property of a vignetting function. Instead of assigning hard constraints, we transform it as soft constraints via an energy term as follows:

$$C_{dec} \equiv \lambda_{dec} \sum_{r=1}^{n-1} \max\left(V(r+1) - V(r), 0\right)^2, \tag{17}$$

where C_{dec} is the non-increasing constraint. The boundary constraint for c_0 prohibits V from being bigger than 1, and is enforced as a hard constraint.

Algorithm 1. Model-based Vignetting Estimation with Outlier Handling

Input: radial bright channel Z^{RB} of an input image
Output: vignetting function V
$c_0 \leftarrow 1$, $f \leftarrow W$, $\{\alpha_i\} \leftarrow 0$ ▷ Initialization
for $iter = 1 : n_{iter}$ **do**
$c_0, f, \{\alpha_i\} \leftarrow$ Estimate the parameters using Eq. (11)
$V \leftarrow$ Reconstruct V using Eqs. (7)-(9)
$w \leftarrow$ Update w with δ using Eq. (18) ▷ Update for outlier handling
$\delta \leftarrow \delta/2$
end for

Iterative Optimization. The energy function in Eq. (11) can be solved with a non-linear constrained optimization method; in this paper, we used the Matlab implementation of trust-region-reflective algorithm [2]. The initial optimization result, however, might be inaccurate due to outliers in Z^{RB} and bad initial parameters, as shown in Fig. 5c. We thus use iterative refinement for more robust estimation of V.

We first optimize Eq. (11) and compute V, setting $\delta = 1$ in Eq. (12). Then, we update $w(r)$ by masking out outlier values of Z^{RB} using the following equation:

$$w(r) = \begin{cases} w(r), & \text{if } \left|c_0 V(r) - Z^{\mathrm{RB}}(r)\right| < \delta \\ 0, & \text{otherwise.} \end{cases}, \tag{18}$$

and halve δ to reject more outliers in the next iteration. The updated parameters δ and $w(r)$, as well as estimated model parameters $\{c_0, f, \{\alpha_i\}\}$, are passed to the next iteration to re-optimize Eq. (11). We iterate this process for 3∼4 times to obtain the final result. Fig. 5d shows an estimated 1D vignetting function.

In Eq. (11), we have several parameters for assigning relative weights between terms although our method is not sensitive to them. In this paper, we fix the parameters as $\lambda_d = \lambda_{dec} = 10^2, \lambda_{c_0} = \lambda_f = 10^{-4}$, and $\lambda_\alpha = 10^{-3}$ for all examples. For initial values of the model parameters, we set $c_0 = 1$, $f = W$, and $\{\alpha_i\} = 0$, where the number of elements in $\{\alpha_i\}$ is 8. Algorithm 1 summarizes our vignetting function estimation algorithm.

It is worth mentioning that the previous single image based methods [15,17] utilize the whole pixels of an image to estimate the vignetting function. In contrast, our estimation algorithm optimizes the vignetting function in the 1D spatial domain with the RBC prior. This strategy greatly reduces the complexity of the estimation algorithm, enabling fast and robust estimation of the vignetting function, despite the complicated energy terms and constraints for the objective function in Eq. (11).

4.3 Restoring the Vignetting-Free Image

Given an estimated V, we recover the vignetting-free image I by dividing $Z(r, \theta)$ with $V(r)$ for all $\theta \in [0, 2\pi)$. Restoring the final image increases the overall

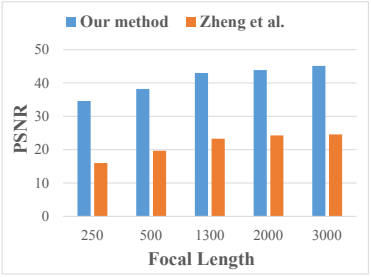

Fig. 6. Comparison with the state-of-the-art single image based method [17] of the mean PSNR values for 100 synthetic examples

brightness of an image, and some pixels of Z containing outliers (e.g., over-exposure and noise) can produce large values. We obtain the final result I as

$$I(r,\theta) = \min\left\{\frac{Z(r,\theta)}{V(r)}, 1\right\}. \tag{19}$$

5 Results

In this section, we validate the effectiveness of our algorithm with various experimental results on synthetic and real images. We implemented our method using Matlab. Our testing environment is a PC running MS Windows 7 64bit version with Intel Core i7 CPU and 12GB RAM.

5.1 Synthetic Examples

To evaluate the performance of our vignetting estimation method, we built a dataset of synthetic images with vignetting effects. We first manually picked up 100 vignetting-free real images which contain indoor/outdoor scenes and complex scene objects (e.g., buildings, humans, animals, trees, grass, cars, sky, sea, etc), and resized each image to have the maximum of image width and height to be 600 pixels. Then we applied five different vignetting functions to each image. The vignetting functions were generated using the extended Kang-Weiss model (Eqs. (7)-(9)), with the five different focal lengths $f \in \{250, 500, 1300, 2000, 3000\}$ while neglecting the geometric factor. Setting the optical center as the image center, total 500 images were generated using Eq. (1). Finally, we compared our method with the state-of-the-art single image vignetting correction method proposed by Zheng et al. [17] using the dataset. The results of Zheng et al. were produced by the authors' implementation.

Fig. 6a shows PSNR values computed between ground truth images and results of each method. Since the effect of vignetting becomes weaker as the focal length increases, results of both methods tend to have higher PSNR values for larger focal lengths. The overall average PSNR value of our results is 40.97, while

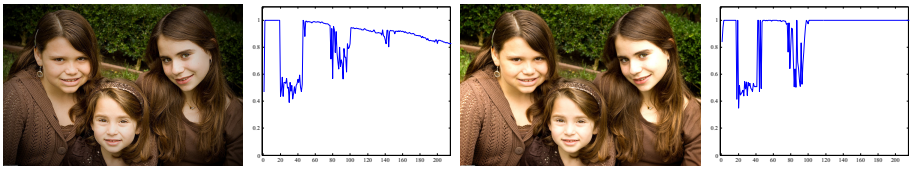

(a) real input image (b) our result

Fig. 7. Real example and its corresponding RBCs

(a) real input (b) Zheng et al. [17] (c) our result

Fig. 8. Comparison with the state-of-the-art method on real photographs

that of Zheng et al. [17] is 21.57. Regardless of the focal length, our method can recover the original vignetting-free image more accurately.

We also estimated the running time of each method with the dataset. The average image size of our synthetic dataset is about 600 by 450 pixels. On average, our method took 1.43 seconds to process one image (i.e., estimating the vignetting function and recovering the corrected image), while Zheng et al.'s algorithm took 21.19 seconds.

5.2 Real Examples

Fig. 7 shows our result on a real example with the corresponding RBCs. As shown in Fig. 7a, the RBC of the input image with vignetting approximately represents the intensity attenuation. Although the image contains complex scene objects such as people and leaf textures, our algorithm recovers a visually pleasing result, making its RBC be a straight line away from the image center.

Fig. 8 shows a comparison with the state-of-the-art single image based method of Zheng et al. [17]. Although Zheng et al.'s approach could remove vignetting from images to a certain degree, vignetting were not fully corrected. In contrast, our method produced better results in terms of visual quality, despite severe vignetting effects in the input. More vignetting correction results on real photographs are included in Fig. 9 and the supplementary material.

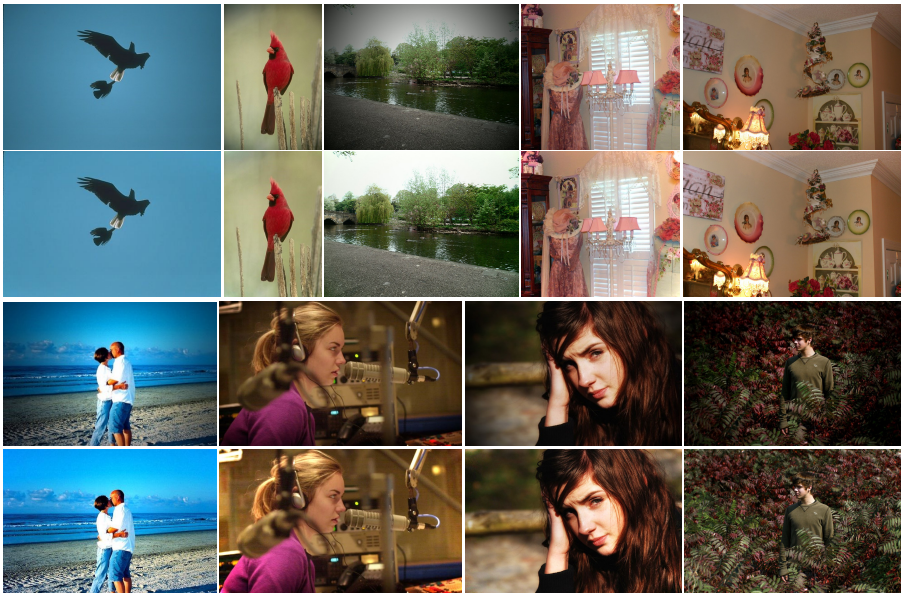

Fig. 9. More vignetting correction results on real photographs. First and third rows show input images containing vignetting, and second and last rows show our results.

5.3 Computation Time

Table 1 summarizes the timing statistics of our method with various image sizes. Even with our unoptimized Matlab implementation, the total running time of our algorithm is about 8.8 seconds for an image of 4000 × 3000 pixels. This is an order of magnitude faster than the state-of-the-art single image vignetting correction method [17], implying the practical usefulness of our method.

Table 1. Timing data with various image sizes

Image size (in pixels)	800 × 600	1,600 × 1,200	3,200 × 2,400	4,000 × 3,000
Computing Z^{RB}	0.27s	0.96s	3.61s	5.52s
Vignetting estimation	1.67s	2.39s	3.27s	2.65s
Final image restoration	0.04s	0.12s	0.45s	0.66s
Total	1.98s	3.47s	7.33s	8.83s

6 Discussion and Future Work

Our RBC prior provides a reliable measure for estimating the vignetting effects of an image. The proposed vignetting estimation algorithm is performed with 1D RBC data instead of 2D image pixels, enabling a high speed of the vignetting correction process. Despite its simplicity, experiments on both synthetic and real images

demonstrate that our method can effectively restore high quality vignetting-free images. The RBC prior is a general image prior which successfully characterizes a statistical property of natural images. We expect it can be adopted for other computer vision and image processing applications than vignetting correction.

Extreme Cases and Limitations. Our RBC prior can capture the vignetting effects even when the illumination is non-uniform, by radially examining image regions and finding radial bright pixels. Still, in extreme cases such as radially non-uniform illumination and combination of non-uniform illumination and different object colors, our vignetting estimation using Eq. (11) may fall into a local minima as the RBC values become unstable. For an image with overall dark colors or low intensities, the RBC prior may not clearly hold. In this case, however, the vignetting itself is not clearly observable as well.

Although our method works well with various types of natural images for vignetting correction, our method may fail on images that do not follow our assumptions. Such cases include arbitrary outliers (e.g., night view and haze), chromatic aberration, or radially asymmetric vignetting effects caused by non-uniform illumination (Fig. 10). In our experiments, we assumed that the optical center corresponds to the image center. This assumption holds in many cases, but it might be broken with cropped images and images taken using special types of lenses. Our method would not produce optimal results for such images.

Future Work. A natural direction for future research will be overcoming the limitations of our method. Utilizing other image priors in conjunction with our RBC prior would enable more accurate and robust estimation of vignetting functions. Exploration of other applications of our RBC prior, such as white balancing, will be definitely interesting future work.

(a) color shading (b) severe cropping

Fig. 10. Limitation examples. For each pair of image, the left is an input and the right is our result. In (a), color shading is emphasized after the vignetting has been removed. In (b), the image has been severely cropped and the optical center is located at the bottom of the image, causing incorrect estimation of the vignetting function.

Acknowledgments. We would like to thank the anonymous reviewers for their constructive comments. We also thank the following flickr users of creative commons license for the photos used in this paper: sagriffin305, Orin Zebest, Dominik Bartsch, Sherry's Rose Cottage, Beth Rankin, Maciek Łempicki, and Andrew Higgins. This work was supported in part by Basic Science Research Program of NRF (2012R1A1A2042837, 2013R1A1A2011692) and Samsung Electronics.

References

1. Asada, N., Amano, A., Baba, M.: Photometric calibration of zoom lens systems. In: Proc. International Conference on Pattern Recognition, vol. 1, pp. 186–190 (1996)
2. Coleman, T., Li, Y.: An interior trust region approach for nonlinear minimization subject to bounds. SIAM Journal on Optimization 6(2), 418–445 (1996)
3. Goldman, D.B.: Vignette and exposure calibration and compensation. IEEE Trans. Pattern Analysis and Machine Intelligence 32(12), 2276–2288 (2010)
4. He, K., Sun, J., Tang, X.: Single image haze removal using dark channel prior. IEEE Trans. Pattern Analysis and Machine Intelligence 33(12), 2341–2353 (2011)
5. Juang, R., Majumder, A.: Photometric self-calibration of a projector-camera system. In: Proc. CVPR, pp. 1–8 (2007)
6. Kang, S.B., Weiss, R.: Can we calibrate a camera using an image of a flat, textureless Lambertian surface? In: Vernon, D. (ed.) ECCV 2000. LNCS, vol. 1843, pp. 640–653. Springer, Heidelberg (2000)
7. Kim, S.J., Pollefeys, M.: Robust radiometric calibration and vignetting correction. IEEE Trans. Pattern Analysis and Machine Intelligence 30(4), 562–576 (2008)
8. Kŏsecká, J., Zhang, W.: Video compass. In: Heyden, A., Sparr, G., Nielsen, M., Johansen, P. (eds.) ECCV 2002, Part IV. LNCS, vol. 2353, pp. 476–490. Springer, Heidelberg (2002)
9. Kuthirummal, S., Agarwala, A., Goldman, D.B., Nayar, S.K.: Priors for large photo collections and what they reveal about cameras. In: Forsyth, D., Torr, P., Zisserman, A. (eds.) ECCV 2008, Part IV. LNCS, vol. 5305, pp. 74–87. Springer, Heidelberg (2008)
10. Litvinov, A., Schechner, Y.: Addressing radiometric nonidealities: A unified framework. In: Proc. CVPR, pp. 52–59 (2005)
11. Lyu, S.: Single image vignetting correction with natural image statistics in derivative domains. In: Proc. ICIP (2010)
12. Sawchuk, A.: Real-time correction of intensity nonlinearities in imaging systems. IEEE Trans. on Computers C-26(1), 34–39 (1977)
13. Yu, W.: Practical anti-vignetting methods for digital cameras. IEEE Trans. on Consumer Electronics 50(4), 975–983 (2004)
14. Zheng, Y., Kambhamettu, C., Lin, S.: Single-image optical center estimation from vignetting and tangential gradient symmetry. In: Proc. CVPR, pp. 2058–2065 (2009)
15. Zheng, Y., Lin, S., Kambhamettu, C., Yu, J., Kang, S.B.: Single-image vignetting correction. IEEE Trans. Pattern Analysis and Machine Intelligence 31(12), 2243–2256 (2009)
16. Zheng, Y., Lin, S., Kang, S.B.: Single-image vignetting correction. In: Proc. CVPR, pp. 461–468 (2006)
17. Zheng, Y., Lin, S., Kang, S.B., Xiao, R., Gee, J.C., Kambhamettu, C.: Single-image vignetting correction from gradient distribution symmetries. IEEE Trans. Pattern Analysis and Machine Intelligence 35(6), 1480–1494 (2013)
18. Zheng, Y., Yu, J., Kang, S.B., Lin, S., Kambhamettu, C.: Single-image vignetting correction using radial gradient symmetry. In: Proc. CVPR, pp. 1–8 (2008)